

Sum-of-products form of the molecular electronic Hamiltonian and application within the MCTDH method

Sudip Sasmal^{1, a)} and Oriol Vendrell^{1, 2, b)}

¹⁾*Theoretische Chemie, Physikalisch-Chemisches Institut, Universität Heidelberg, Im Neunheimer Feld 229, 69120 Heidelberg, Germany*

²⁾*Interdisciplinary Center for Scientific Computing, Universität Heidelberg, Im Neunheimer Feld 205, 69120 Heidelberg, Germany*

(Dated: 8 September 2022)

We introduce two different approaches to represent the second-quantized electronic Hamiltonian in a sum-of-products form. These procedures aim at mitigating the quartic scaling of the number of terms in the Hamiltonian with respect to the number of spin orbitals, and thus enable applications to larger molecular systems. Here we describe the application of these approaches within the multi-configuration time-dependent Hartree framework. This approach is applied to the calculation of eigen energies of LiH and electronic ionization spectrum of H₂O.

I. INTRODUCTION

The multiconfiguration time-dependent Hartree (MCTDH)^{1–5} and its multilayer generalization (ML-MCTDH)^{6–10} are very efficient methods to simulate high dimensional quantum dynamics of nuclear degrees of freedom. In its original form, the MCTDH Ansatz cannot describe a system of indistinguishable particles as it assumes a product form of the underlying SPFs and thus, does not reflect the proper symmetry of the indistinguishable particles. However, one can construct the multiconfiguration wavefunction in the basis of Slater determinants and permanents to treat systems of fermions and bosons, respectively. These theories are called MCTDH for fermions (MCTDH-F)^{11–15} and bosons (MCTDH-B)^{12,16}. A unified version of the two theories using a non-symmetric core tensor to connect mixtures of different types of indistinguishable particles has also been established¹⁷. A limitation of such descriptions is that the number of configurations of the electronic/bosonic subsystem increases combinatorially with the number of particles and single-particle functions, while the antisymmetry/symmetry requirement prevents their further decomposition into smaller-rank tensors. Hence, within the same type of indistinguishable particle, MCTDH-B and MCTDH-F approaches are incompatible with the multilayer extension of the MCTDH framework.

A fundamentally different alternative to describe systems of indistinguishable particles is to use the second quantization representation. Wang and Thoss described and applied this approach in the context of MCTDH and called it MCTDH in SQR (MCTDH-SQR)¹⁸. Here, the state of the system is described in the occupation number representation referring to the occupation of a given set of spin-orbitals. The symmetry of the indis-

tinguishable particles is encoded in the creation and annihilation operators acting on the state of the system. In this approach, as the coordinates are the occupation of individual spin-orbitals, the DOFs are distinguishable and hence a multilayer Ansatz of the wavefunction is straightforward. This approach has been used in a number of applications after its introduction, e.g. to solve the impurity problem that appears in non-equilibrium dynamical mean-field theory¹⁹, quantum transport in molecular junctions^{20–22} and quantum dots^{23,24}. Manthe and Weike developed an MCTDH-SQR approach based on time-dependent optimal (spin-)orbitals, the MCTDH-oSQR method^{25,26}. The aforementioned applications were concerned with model Hamiltonians^{18–26}. Recently, we extended the MCTDH-SQR method to describe the non-adiabatic dynamics in molecular systems based on the second-quantized representation of the electrons and first-quantized representation of the nuclear coordinates while providing expressions for the non-adiabatic coupling matrix elements in this combined representation²⁷. In this formalism, most non-adiabatic effects are described by the time-evolution of the electronic subsystem coupled to the dynamics of the nuclei and bypasses the explicit calculation of non-adiabatic couplings in terms of electronic states. Thus, the approach provides an alternative to the usual group BO approximation.

However, the major problem of the MCTDH-SQR method applied to *ab initio* studies of large molecular systems remains the enormous size of the electronic SQR Hamiltonian, whose number of terms increases with the fourth power of the number of spin-orbitals. The density matrix renormalization group (DMRG)^{28–30} formalism, which is based on a similar tensor representation compared to ML-MCTDH, avoids such scaling by representing the Hamiltonian as matrix product operator (MPO)^{31–36} that matches the matrix product state (MPS)^{31,33} structure of the wavefunction. A comparably compact form of the electronic Hamiltonian based on a sum-of-products (SOP) expansion, which is able to regain the maximum performance from the multiconfigurational form of the MCTDH wavefunction, has not yet been put

^{a)}e-mail: sudip.sasmal@pci.uni-heidelberg.de

^{b)}e-mail: oriol.vendrell@pci.uni-heidelberg.de

forward. In comparison, for the nuclear dynamics problem, there exist a plethora of methods to bring general potential energy surfaces to a SOP form, including the POTFIT^{3,37,38}, multigrid POTFIT³⁹, Monte Carlo POTFIT⁴⁰ and its multilayer variant⁴¹, multilayer POTFIT⁴², Monte Carlo CANDECOMP⁴³ algorithms and neural network approaches⁴⁴⁻⁵⁰.

In this work, we introduce and benchmark two SOP-based strategies that aim at mitigating the quartic scaling of the electronic Hamiltonian with respect to the number of spin-orbitals. The paper is organized as follows. Section II A reviews the general strategy to write the SQR electronic Hamiltonian in SOP form. Section II B discusses the choice of DOF in the MCTDH-SQR formalism and Section II C introduces two strategies that lead to compact SOP forms of the electronic SQR Hamiltonian. Secs III A and III B present and discuss numerical results of the LiH and H₂O systems, respectively. Finally a summary and conclusions are provided in Section IV.

II. THEORY

A. Sum-of-products form of the electronic Hamiltonian

The molecular electronic Hamiltonian in the second quantization framework reads

$$\hat{H} = \sum_{ij} h_{ij} \hat{a}_i^\dagger \hat{a}_j + \frac{1}{2} \sum_{ijkl} v_{ijkl} \hat{a}_i^\dagger \hat{a}_j^\dagger \hat{a}_l \hat{a}_k, \quad (1)$$

where

$$h_{ij} = \langle \phi_i(1) | -\frac{1}{2} \nabla_1^2 - \sum_{A=1}^M \frac{Z_A}{r_{1A}} | \phi_j(1) \rangle, \quad (2)$$

$$v_{ijkl} = \langle \phi_i(1) \phi_j(2) | \frac{1}{r_{12}} | \phi_k(1) \phi_l(2) \rangle, \quad (3)$$

are the one- and two-body integrals, involving the spin orbitals ϕ_i , respectively. The \hat{a}_i and \hat{a}_i^\dagger correspond to the annihilation and creation operators that annihilates and creates an electron in the i -th spin orbitals, respectively, satisfy the fermionic commutation relations

$$\{\hat{a}_i, \hat{a}_j^\dagger\} = \hat{a}_i \hat{a}_j^\dagger + \hat{a}_j^\dagger \hat{a}_i = \delta_{ij}, \quad (4)$$

$$\{\hat{a}_i^\dagger, \hat{a}_j^\dagger\} = \{\hat{a}_i, \hat{a}_j\} = 0. \quad (5)$$

Although the electronic Hamiltonian written in Eq. 1 looks like already being in a SOP form, the anti-commutation relations of the fermionic creation and annihilation operators in Eq. 4 lead to the accumulation of a phase factor $S_s = \sum_{k=1}^{s-1} n_k$ depending on the occupation of all spin-orbitals before the s -th position for \hat{a}_s acting on a Fock-space configuration (the same is true for \hat{a}_s^\dagger)⁵¹

$$\begin{aligned} \hat{a}_s |n_1, n_2, \dots, n_M\rangle &= \hat{a}_s (\hat{a}_1^\dagger)^{n_1} (\hat{a}_2^\dagger)^{n_2} \dots (\hat{a}_M^\dagger)^{n_M} |0\rangle \\ &= (-1)^{S_s} (\hat{a}_1^\dagger)^{n_1} (\hat{a}_2^\dagger)^{n_2} \dots (\hat{a}_s \hat{a}_s^\dagger) \dots (\hat{a}_M^\dagger)^{n_M} |0\rangle. \end{aligned} \quad (6)$$

This phase factor complicates the application of Hamiltonian (Eq. 1) to the wavefunction. Clearly, the operator $\hat{a}_s^{(\dagger)}$ acts beyond its index s and therefore the electronic SQR Hamiltonian, in general, is not in the SOP form with respect to the primitive degrees of freedom. Wang and Thoss solved this issue by mapping the fermionic operators onto equivalent spin operators¹⁸. Formally, this mapping consists in applying the inverse Jordan-Wigner (JW) transformation to the fermionic field operators and effectively transforming the fermionic Hamiltonian into an equivalent spin-chain Hamiltonian⁵². The equivalent spin-1/2 chain Hamiltonian after the JW transformation reads²⁷

$$\begin{aligned} \hat{H} &= \sum_{ij} h_{ij} \left(\prod_{q=a+1}^{b-1} \hat{\sigma}_q^z \right) \hat{\sigma}_i^+ \hat{\sigma}_j^- \\ &+ \frac{1}{2} \sum_{ijkl} v_{ijkl} \left(\prod_{q=a+1}^{b-1} \hat{\sigma}_q^z \prod_{q'=c+1}^{d-1} \hat{\sigma}_{q'}^z \right) \\ &\text{sgn}(j-i) \text{sgn}(l-k) \hat{\sigma}_i^+ \hat{\sigma}_j^+ \hat{\sigma}_l^- \hat{\sigma}_k^-. \end{aligned} \quad (7)$$

where $\hat{\sigma}_i^+ = \frac{1}{2} (\hat{\sigma}_i^x + i \hat{\sigma}_i^y)$, $\hat{\sigma}_i^- = \frac{1}{2} (\hat{\sigma}_i^x - i \hat{\sigma}_i^y)$, and $\hat{\sigma}_k^z$ are the standard spin ladder operators with Pauli matrices σ^x , σ^y and σ^z . Here the indices (a, b, c, d) correspond to the (i, j, k, l) indices, but ordered from smaller to larger and the sgn function is defined as

$$\text{sgn}(x) = \begin{cases} 1, & \text{if } x \geq 0 \\ -1, & \text{otherwise.} \end{cases} \quad (8)$$

The operators $\hat{\sigma}_\kappa^+$, $\hat{\sigma}_\kappa^-$ and $\hat{\sigma}_\kappa^z$ acts locally on κ -th spin- $\frac{1}{2}$ basis function and their matrix representation reads

$$\sigma^+ = \begin{pmatrix} 0 & 0 \\ 1 & 0 \end{pmatrix}; \quad \sigma^- = \begin{pmatrix} 0 & 1 \\ 0 & 0 \end{pmatrix}; \quad \sigma^z = \begin{pmatrix} 1 & 0 \\ 0 & -1 \end{pmatrix}. \quad (9)$$

Clearly, the electronic Hamiltonian written in Eq. 7 is in the SOP form with respect to the primitive DOFs (spin- $\frac{1}{2}$ basis).

B. DOF in MCTDH-SQR: Spin and Fock space

In the MCTDH-SQR formalism for fermionic system (without mode combination), there are two limiting wavefunction Ansatz: Each spin degree of freedom (S-DOF) is described by either (i) one or (ii) two time-dependent SPFs. The former corresponds to a time dependent Hartree (TDH) wavefunction with a single Hartree product and the latter corresponds to the exact wavefunction consisting of 2^M configurations, where M is the number of S-DOF. Thus, the limiting case (i) leads to a poor description of correlated state and the later leads to an exact formulation, which becomes quickly unaffordable as the number of S-DOF (i.e., spin orbitals) increases. Therefore, the only practical way to apply the MCTDH-SQR method is to create groups of S-DOFs,

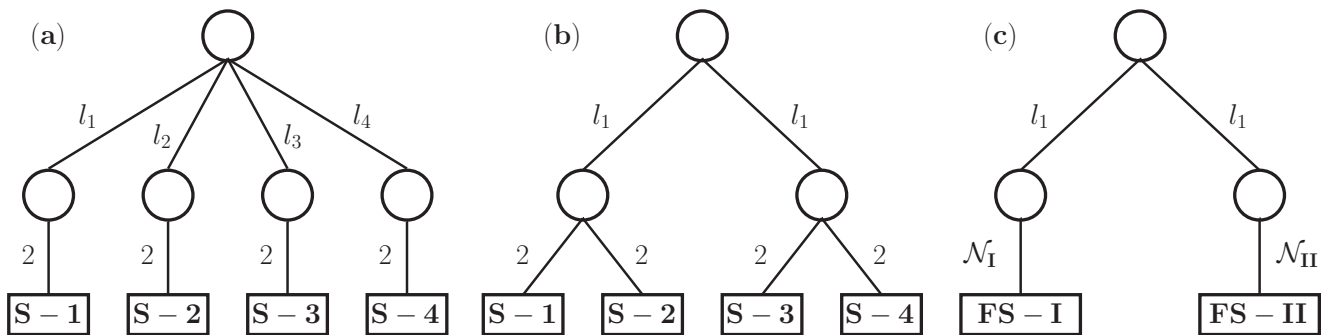


FIG. 1. Tree structures for the MCTDH-SQR wavefunction containing four spin orbitals: (a) Normal MCTDH wavefunction tree, in which spin degree of freedoms (S-DOF) are considered as primitive DOFs. (b) MCTDH wavefunction tree with mode combination, in which S-DOFs are considered as primitive DOFs. (c) MCTDH wavefunction tree, in which the Fock space of two spin orbitals is considered as single DOF (FS-DOF). l_κ denotes number of SPF of the κ -th mode and \mathcal{N}_κ is the number of configuration of κ -th FS-DOF.

either through mode combination or through its multi-layer generalization. Figures 1 (a) and (b) show the normal MCTDH wavefunction and the MCTDH wavefunction with mode combination, respectively, where S-DOFs are used as primitive DOFs.

For M spin orbitals there are 2^M Fock states. On the other hand one can divide the total Fock space into f sub-Fock spaces by grouping the M spin orbitals into f groups (m_1, m_2, \dots, m_f)

$$\mathcal{F}(M) = \mathcal{F}_1(m_1) \otimes \mathcal{F}_2(m_2) \otimes \dots \otimes \mathcal{F}_f(m_f) \quad (10)$$

where $\mathcal{F}_\kappa(m_\kappa)$ denotes the sub-Fock space of the κ -th FS-DOF (consists of m_κ S-DOFs) with 2^{m_κ} Fock states and

$$M = \sum_{\kappa=1}^f m_\kappa. \quad (11)$$

Now, one can represent the configurations of the sub-Fock space $\mathcal{F}_\kappa(m_\kappa)$ as a new primitive DOF. We refer to this representation of the primitive DOF as Fock space DOF (FS-DOF). Fig. 1 (c) shows the MCTDH wavefunction involving FS-DOF as primitive DOF. In the FS-DOF formalism, one needs to transform the primitive operator string described in the Eq. 7 into new primitive matrix operators acting onto the sub-Fock spaces of their corresponding FS-DOF.

In the FS-DOF representation, the state of the system is described by kets $|i_1, \dots, i_f\rangle$, where i_κ corresponds to the i -th configuration of the κ -th FS-DOF. One can think of the i_κ configuration indices as indexing Euclidean basis vectors within each degree of freedom. The configurations within a FS-DOF can correspond, in general, to different electron occupation numbers. A matrix element of the total Hamiltonian is then represented as

$$H_{z_1, \dots, z_f} = H_{i_1, \dots, i_f}^{j_1, \dots, j_f} = \langle j_1, \dots, j_f | \hat{H} | i_1, \dots, i_f \rangle, \quad (12)$$

where $z_\kappa = (i_\kappa, j_\kappa)$ are double indices indicating the bra- and ket-side configurations within each FS-DOF. This electronic Hamiltonian is very sparse and, clearly, it can only be explicitly constructed and diagonalized for small systems. In the following, thus, we will discuss the construction of sum-of-product (SOP) forms of Hamiltonian (12), either exact or approximate, and their use within the framework of MCTDH-SQR.

C. Compact form of the Hamiltonian in the FS-DOF basis

The number of terms of the electronic SQR Hamiltonian (Eqs. 1, 7) increases with M^4 where M is the total number of spin orbitals under consideration. One can only reduce the number of terms by applying cutoffs to different types of one- and two-electron integrals at the expense reducing the accuracy of the Hamiltonian²⁷. In the following, we formulate two strategies to reduce the number of Hamiltonian terms in the SOP form of the Hamiltonian. Both strategies are based on the formation of FS-DOF as the primitive DOF and therefore in both strategies the MCTDH wavefunction structure remains the same. The difference is in the way the Hamiltonian is constructed, either (i) directly starting from the original SQR Hamiltonian and mapping each product term (each chain of spin operators) to its matrix representation in the FS-DOF basis or (ii) constructing the matrix elements of the product operator directly as an optimal SOP fit to the full operator.

1. Summed SQR Hamiltonian: S-SQR

As a starter, the number of terms of the SQR Hamiltonian in its spin- $\frac{1}{2}$ (S-DOF) form, Eq. 7, can be reduced by summing up those two-body terms that can be transformed into the same order of the ladder operators. In

other words, one should use the symmetry of the four-index tensor v_{ijkl} to avoid unnecessary work when applying the operator. The 2-index correlated operators that can be added together are

$$v_{ijij}\hat{a}_i^\dagger\hat{a}_j^\dagger\hat{a}_j\hat{a}_i + v_{ijji}\hat{a}_i^\dagger\hat{a}_j^\dagger\hat{a}_i\hat{a}_j = (v_{ijij} - v_{ijji})\hat{a}_i^\dagger\hat{a}_j^\dagger\hat{a}_j\hat{a}_i. \quad (13)$$

The 3-index correlated operators that can be added together are

$$\begin{aligned} & v_{ijik}\hat{a}_i^\dagger\hat{a}_j^\dagger\hat{a}_k\hat{a}_i + v_{ijkj}\hat{a}_i^\dagger\hat{a}_j^\dagger\hat{a}_k\hat{a}_i + \\ & v_{jikj}\hat{a}_i^\dagger\hat{a}_j^\dagger\hat{a}_k\hat{a}_i + v_{jiki}\hat{a}_i^\dagger\hat{a}_j^\dagger\hat{a}_k\hat{a}_i \\ & = (v_{ijik} - v_{ijkj} + v_{jikj} - v_{jiki})\hat{a}_i^\dagger\hat{a}_j^\dagger\hat{a}_k\hat{a}_i. \end{aligned} \quad (14)$$

The 4-index correlated operators that can be added together are

$$\begin{aligned} & v_{ijkl}\hat{a}_i^\dagger\hat{a}_j^\dagger\hat{a}_l\hat{a}_k + v_{ijlk}\hat{a}_i^\dagger\hat{a}_j^\dagger\hat{a}_l\hat{a}_k + \\ & v_{jilk}\hat{a}_i^\dagger\hat{a}_j^\dagger\hat{a}_l\hat{a}_k + v_{jikl}\hat{a}_i^\dagger\hat{a}_j^\dagger\hat{a}_l\hat{a}_k \\ & = (v_{ijkl} - v_{ijlk} + v_{jilk} - v_{jikl})\hat{a}_i^\dagger\hat{a}_j^\dagger\hat{a}_l\hat{a}_k. \end{aligned} \quad (15)$$

However, the reduction in the number of terms achieved by the sums in Eqs. 13, 14 and 15 is negligible compared to the number of terms in the SQR Hamiltonian. The situation improves substantially while using FS-DOF as primitive DOF. In the FS-DOF primitive basis, all terms (both one- and two-body) that act only within the spin-orbitals of one FS-DOF can be summed up to form an uncorrelated operator term. Similarly, one can form correlated operators (products acting on two or more FS-DOF) by summing all terms that act within one FS-DOF for each distinct string operating on the spin orbitals of the other FS-DOF.

For example, for the FS-DOF construction described in Fig. 1, one can form the uncorrelated operator of the 1st FS-DOF (FS-I) by summing up the following terms

$$\begin{aligned} & h_{11}(\hat{a}_1^\dagger\hat{a}_1)^{(I)} + h_{12}(\hat{a}_1^\dagger\hat{a}_2)^{(I)} + h_{21}(\hat{a}_2^\dagger\hat{a}_1)^{(I)} + h_{22}(\hat{a}_2^\dagger\hat{a}_2)^{(I)} \\ & + v_{1212}(\hat{a}_1^\dagger\hat{a}_2^\dagger\hat{a}_2\hat{a}_1)^{(I)} + v_{1221}(\hat{a}_1^\dagger\hat{a}_2^\dagger\hat{a}_1\hat{a}_2)^{(I)}. \end{aligned} \quad (16)$$

Of course, one needs to transform the fermionic operator strings into spin operators using the JW transformation and then form the matrix operator of the corresponding chain of operators in the space of the FS-DOF before the summation operation. One of the correlated operator terms can be formed by summing up the following contributions

$$\begin{aligned} & h_{13}\hat{a}_1^\dagger\hat{a}_3 + h_{23}\hat{a}_2^\dagger\hat{a}_3 = h_{13}\hat{\sigma}_1^+\hat{\sigma}_2^z\hat{\sigma}_3^- + h_{23}\hat{\sigma}_2^+\hat{\sigma}_3^- \\ & = \left(h_{13}(\hat{\sigma}_1^+\hat{\sigma}_2^z)^{(I)} + h_{23}(\hat{\sigma}_2^+)^{(I)} \right) (\hat{\sigma}_3^-)^{(II)}. \end{aligned} \quad (17)$$

Please note that there are other two-body terms that can also be added to the terms described in Eq. 17, for example, v_{1213} , v_{1231} , v_{2131} , v_{2113} , v_{2123} , v_{2132} , v_{1232} , and

v_{1223} terms associated with their corresponding operator string. The compact form of SQR Hamiltonian for an arbitrary FS-DOF combination is given in Appendix A.

The S-SQR form of the Hamiltonian is exact within the space of configurations spanned by the different FS-DOF. Since the matrix operators acting on each FS-DOF and for different products are not related to each other, this form of the SQR operator corresponds to an exact canonical polyadic decomposition (CANDECOMP)^{43,53–56} In general, it reads

$$H_{z_1, \dots, z_f} = \sum_{s=1}^R \prod_{\kappa=1}^f [\mathbf{X}_s^{(\kappa)}]_{z_\kappa}, \quad (18)$$

where any multiplicative constants are absorbed into the matrices. The final rank R , and hence the degree of compactification of the Hamiltonian, depends on the grouping of the orbitals to form the FS-DOF. In the limiting case that all spin orbitals are grouped together to form just one FS-DOF, $R = 1$. This is not very useful as the size of the only operator matrix is $2^M \times 2^M$ and corresponds to the full configuration interaction Hamiltonian in Fock space. In the case that no grouping is performed (e.g. in a ML-MCTDH calculation without mode-combination) the Hamiltonian remains identical with the original SQR Hamiltonian and no gain through summation is achieved.

2. Tucker decomposition of the SQR Hamiltonian: T-SQR

An alternative approach to a SOP form abandons the exact representation of the Hamiltonian and introduces an optimal Tucker decomposition of the electronic SQR Hamiltonian H_{z_1, \dots, z_f} in the FS-DOF primitive basis,

$$H_{z_1, \dots, z_f}^{(T)} \approx \sum_{l_1}^{n_1} \cdots \sum_{l_f}^{n_f} g_{l_1, \dots, l_f} \prod_{\kappa=1}^f [\mathbf{O}^{(\kappa, l_\kappa)}]_{z_\kappa}, \quad (19)$$

where g_{l_1, \dots, l_f} are the elements of the Tucker core tensor with rank (n_1, n_2, \dots, n_f) and $\mathbf{O}^{(\kappa, l_\kappa)}$ is the l_κ -th single particle operator (SPO) acting of the κ -th FS-DOF. The operator matrices $\mathbf{O}^{(\kappa, l_\kappa)}$ are defined in the sub-Fock space $(\mathcal{F}_\kappa(m_\kappa))$ formed by the κ -th FS-DOF. When multiplied as vectors, these elements form an orthonormal set,

$$\sum_{z_\kappa} [\mathbf{O}^{(\kappa, l_\kappa)}]_{z_\kappa} \cdot [\mathbf{O}^{(\kappa, p_\kappa)}]_{z_\kappa} = \delta_{l_\kappa, p_\kappa}. \quad (20)$$

The challenge here is to obtain the core tensor g and the basis of SPO matrices. Similarly to the original POTFIT^{3,37,38} algorithm for multidimensional potential energy surfaces, this can be formulated as the numerical problem of finding optimal coefficients with respect to the minimization of some error function. One of such

error function is the sum of squared errors

$$\mathcal{L}^2 = \sum_{z_1} \cdots \sum_{z_f} \left(H_{z_1, \dots, z_f} - H_{z_1, \dots, z_f}^{(T)} \right)^2 \quad (21)$$

where $H_{z_1, \dots, z_f}^{(T)}$ takes the form of Eq. (19).

The Hamiltonian tensor elements H_{z_1, \dots, z_f} entering Eq. (21) can be evaluated either directly using the Slater-Condon rules in the full configuration space^{57,58}, or by using the representation of Eq. (18). The rank of the original Hamiltonian tensor is $\prod_{\kappa} \mathcal{N}_{\kappa}^2 = 2^{2M}$. Since, the Tucker rank ($\prod_{\kappa} n_{\kappa}$) is, in general, much smaller than the rank of the original Hamiltonian, the Tucker decomposed Hamiltonian can easily achieve a more compact form compared to the original Hamiltonian tensor. Nonetheless, the rank of the SQR Hamiltonian in the full Fock space scales much more rapidly than M^4 , although its matrix representation is extremely sparse. It is therefore yet to be tested numerically whether an optimal Tucker representation of the operator can bring an advantage compared to the previously introduced, exact summation strategy.

The rank of the Hamiltonian in Eq. 19 in the SOP form, $\prod_{\kappa} n_{\kappa}$ can still be reduced by a factor of n_{ν} , where ν is the index of any of the FS-DOFs, by contracting this degree of freedom with the core tensor and summing up all operators of the ν FS-DOF that multiply a common string of operators in the other FS-DOFs. This operation is standardly performed in the POTFIT algorithm for potential operators.

In practice, we have used the `TensorLy`⁵⁹, python library that uses higher-order orthogonal iteration (HOOI)⁶⁰ to obtain the Tucker decomposition of the electronic Hamiltonian. As in the original potfit algorithm, the full tensor needs to be stored in memory, which prevents the application of this approach to large molecular systems where the original tensor cannot be stored in memory. We are not concerned with this limitation for the proof-of-concept application to molecular electronic dynamics, and will address it in future work resorting, e.g., to sampling strategies over the elements of the primitive tensor^{40,43}.

Finally, we note that the Tucker decomposed Hamiltonian obtained by numerically minimizing the error function (Eq. 21) is not completely Hermitian, as Hermiticity of the product terms is not explicitly enforced in the fitting form. This results in small numerical inaccuracies related to norm conservation of the wavefunction. Hermiticity can be restored, e.g., if the space of SPOs within each FS-DOF is spanned by Hermitian matrices $\mathbf{A}^{(\kappa, j_{\kappa})} = \mathbf{A}^{\dagger(\kappa, j_{\kappa})}$ and by pairs of Hermitian conjugate matrices $\mathbf{B}^{(\kappa, j_{\kappa})}$, $\mathbf{B}^{\dagger(\kappa, j_{\kappa})}$. Non-Hermitian SPOs are crucial for representing the electronic dynamics across different FS-DOF (in a similar way as the original creation and annihilation operators) but each term containing $\mathbf{B}^{(\kappa, j_{\kappa})}$ must be matched by a corresponding term with the same core-tensor coefficient and containing $\mathbf{B}^{\dagger(\kappa, j_{\kappa})}$. Instead

of enforcing these constraints during the minimization of \mathcal{L}^2 , which is more efficient, currently we opted for reintroducing Hermiticity a posteriori. To this end we average each product term in Eq 19 with its Hermitian conjugate, thus turning the Hamiltonian exactly Hermitian with a factor 2 more terms.

3. Pruning of the FS-DOF sub-Fock space

As a final remark, grouping the primitive S-DOF as FS-DOF allows for each sub-Fock space to be statically pruned by restricting the number of electrons and/or by removing configurations with unwanted orbital occupation. This is equivalent of removing undesired grid points from a multidimensional grid in a discrete variable representation. As an example, let us consider a system containing two FS-DOF each containing four spin orbitals. The number of configurations (\mathcal{N}) in each FS-DOF is $2^4 = 16$. Let's also consider the system contains four electrons and the orbitals are energetically ordered with respect to a pre-existing first quantization mean-fields calculation. So, the lowest energy configuration is where all the orbitals are occupied ($|1, 1, 1, 1\rangle$) in the 1st FS-DOF and all the orbitals in the 2nd FS-DOF are empty ($|0, 0, 0, 0\rangle$). Now, if one allows only up to two holes in the 1st FS-DOF and two particles in the 2nd FS-DOF, the number of configurations in each FS-DOF shrinks from 16 to 11. One can further removed the configuration of the 1st FS-DOF where both of the lowest two spin orbitals are empty by removing ($|0, 0, 1, 1\rangle$) if chemically irrelevant and shrinks the number of configurations (\mathcal{N}_1) to 10. Similarly, if chemically irrelevant, one can further remove the $|0, 0, 1, 1\rangle$ occupation number state from the 2nd FS-DOF to shrink the number of configurations (\mathcal{N}_2) to 10. The pruning of the FS-DOF allows one to reduce the primitive space of the FS-DOF without compensating too much chemical accuracy. Another advantage of the (pruned) FS-DOF representation is that the SQR operators acting on the SPFs of the corresponding FS-DOF are very sparse and correspond to mappings (see Appendix B) that can lead to large efficiency gain in computations.

III. RESULTS AND DISCUSSION

A. Electronic eigenenergies of LiH

We have calculated the adiabatic electronic energies of LiH by applying the MCTDH-SQR method to the electronic SQR Hamiltonian at fixed nuclear geometries. The 6-31G atomic basis is used for both Li and H. In first quantization, the potential energy curves (PECs) of the lowest four electronic states are obtained for comparison at the full configuration interaction level. In SQR, the PECs are obtained through the propagation of an

TABLE I. Number of Hamiltonian terms, memory required to store the operator matrices and wall-clock time for the different representation of Hamiltonian. The wall-clock time is given for 1 fs time propagation. The calculations have been performed with 14 CPUs using shared-memory parallelization on the same machine and CPU type, namely, Dual-Core Intel Xeon, processor type E5-2650 v2 running at 2.6 GHz and the wall-clock times are intended for their relative comparison only. Matrix and mapping correspond to usual and mapping strategy (see Appendix B, Algorithm 1) used for the matrix vector multiplication, respectively. Maximum rank of the T-SQR Hamiltonian is (6241, 6241)

Method	Hamil. terms	Size	Time (h:m)
SQR			
mapping	16138	465 KB	7:14
S-SQR			
matrix	2003	394 MB	1:43
mapping	2003	5 MB	1:19
T-SQR			
(20, 20)	40	703 KB	0:01
(40, 40)	80	1.3 MB	0:01
(60, 60)	120	2.5 MB	0:01
(80, 80)	160	3.1 MB	0:02
(100, 100)	200	3.6 MB	0:02
(150, 150)	300	4.7 MB	0:03

MCTDH-SQR wavefunction which overlaps with the various excited electronic states. The initial condition for the singlet states is

$$|\Psi(t=0)\rangle = |1_\alpha, 1_\beta, 2_\alpha, 2_\beta\rangle + |1_\alpha, 1_\beta, 2_\alpha, 3_\beta\rangle - |1_\alpha, 1_\beta, 2_\beta, 3_\alpha\rangle, \quad (22)$$

and for the triplet states is

$$|\Psi(t=0)\rangle = |1_\alpha, 1_\beta, 2_\alpha, 3_\beta\rangle + |1_\alpha, 1_\beta, 2_\beta, 3_\alpha\rangle + |1_\alpha, 1_\beta, 2_\alpha, 6_\beta\rangle + |1_\alpha, 1_\beta, 2_\beta, 6_\alpha\rangle. \quad (23)$$

The wavefunction in Eqs. (22) and (23) is spin-singlet and spin-triplet and overlaps with the desired $^1\Sigma^+$ and $^3\Sigma^+$ states, respectively. The electronic eigenenergies are obtained from the maxima of the peaks in the power spectrum obtained from the Fourier transform of the autocorrelation function

$$\sigma(E) = \frac{1}{\pi} \text{Re} \int_0^\infty e^{iEt} \langle \Psi | \Psi(t) \rangle dt. \quad (24)$$

The FS-DOFs for the SQR calculations are grouped in the following way. The lowest 5 spatial (10 spin) molecular orbitals are arranged into the first FS-DOF and the remaining 6 spatial (12 spin) molecular orbitals into the second FS-DOF. This results in 2^{10} and 2^{12} configurations in the first and second FS-DOF, respectively.

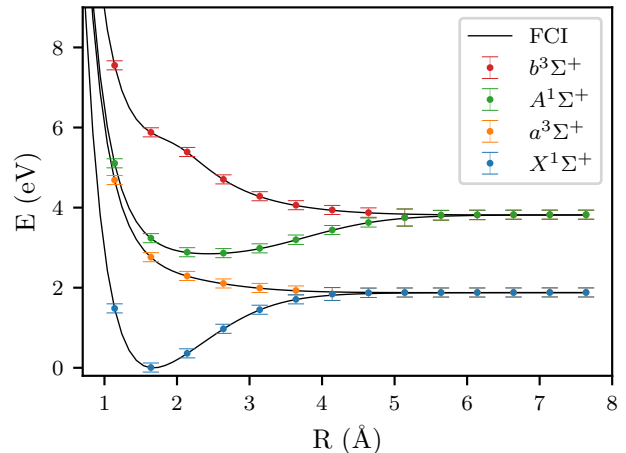


FIG. 2. Comparison of eigenenergies of S-SQR Hamiltonian with FCI.

These Fock subspaces are then pruned using the following procedure. (i) In the first FS-DOF we allow (0–2) alpha, (0–2) beta and (2–4) total electrons. We further prune this FS-DOF by removing all configurations where the lowest energy MOs (1s of Li) are completely empty (i.e. both alpha and beta electrons missing from this spatial orbital). This shrinks the number of configurations of this FS-DOF from 1024 to 133. (ii) Similarly in the second FS-DOF, we allow (0–2) alpha, (0–2) beta and (0–2) total electrons. This shrinks the number of configurations of this FS-DOF from 4096 to 79.

The electronic SQR Hamiltonian is represented either in S-SQR or T-SQR forms. Table I compares the number of Hamiltonian terms, memory required to store the operator matrices and CPU time for different calculations in each of the two approaches. For S-SQR Hamiltonian, we have compare calculations where the matrices of each Hamiltonian terms are stored (and thus, applied to the wavefunction) as a matrix or as a mapping (see Appendix B). For the mapping case, we consider in turn two situations – (i) the original SQR Hamiltonian is applied without summing the uncorrelated and correlated terms, (ii) the Hamiltonian terms are compacted as much as possible to form S-SQR Hamiltonian and then applied to the wavefunction. For the operator in matrix form, the MCTDH code⁶¹ by default sums up the Hamiltonian terms. From the Table I, it is clear that the uncompact (mapping) form of the Hamiltonian is the slowest. On the other hand, the compacted S-SQR Hamiltonian using the mapping for the matrix-vector multiplications is fastest and requires less memory compared to the S-SQR Hamiltonian matrix form. Note that with identical MCTDH parameters, all of the three calculations yield identical results within numerical accuracy. The electronic eigenenergies in the spin orbital basis along with the PECs obtained from the FCI calculation are shown in Fig. 2.

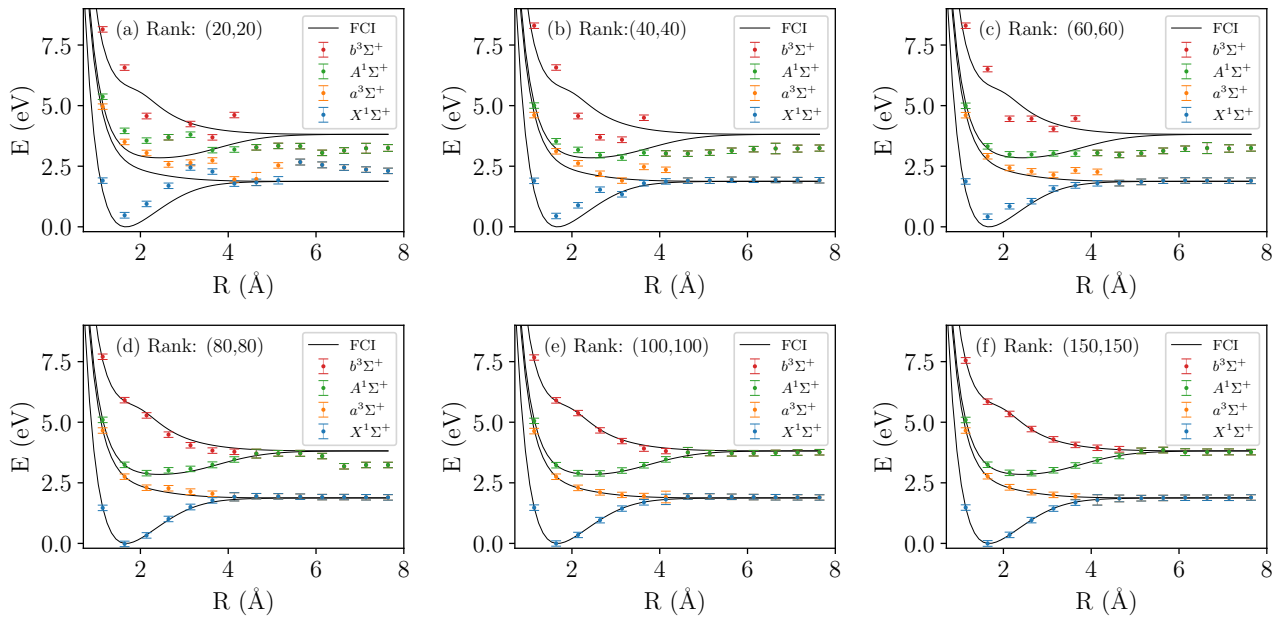


FIG. 3. Comparison of electronic eigenenergies in the T-SQR Hamiltonian approach. Electronic eigenenergies calculated with Tucker rank (20,20), (40,40), (60,60), (80,80), (100,100) and (150,150) are shown in (a), (b), (c), (d), (e) and (f), respectively. Maximum rank of the T-SQR Hamiltonian is (6241,6241). Black lines are the potential energy curves calculated in the FCI method.

Next, we compare the electronic Hamiltonian in the T-SQR Hamiltonian approach. In Table I, the number of Hamiltonian terms, memory required to store the operator matrices and CPU time are compared as a function of the rank of the Tucker decomposition. The calculated eigenenergies for different Tucker rank are shown in Fig. 3. As expected, the electronic energies are gradually improving with increasing Tucker rank. This is illustrated in Fig. 4, where we show the convergence of the eigenenergies ($\Delta E = E_{FCI} - E_{T-SQR}$) at the equilibrium geometry (at $R = 1.64 \text{ \AA}$) with respect to the Tucker rank. A very good convergence is achieved with a Tucker rank (100,100), much smaller than the full rank (6241, 6241). For this small example using the T-SQR Hamiltonian approach, the execution time for the converged calculation of comparable accuracy is ~ 26 times faster (cf. Table I) than the best possible compact form of the S-SQR Hamiltonian approach. This is in part achieved because of the contraction of the operator for one of the two FS-DOFs.

B. Electronic ionization spectrum of H_2O

The *ab initio* MCTDH-SQR approach can be directly applied to the calculation of ionization spectra of molecular systems through time-propagation instead of matrix diagonalization. Here we benchmark the method on the water molecule. The 6-31G atomic basis is used for both O and H to generate the MOs of H_2O . The lowest energy MO (1s of O) is frozen and the remaining 12 spatial

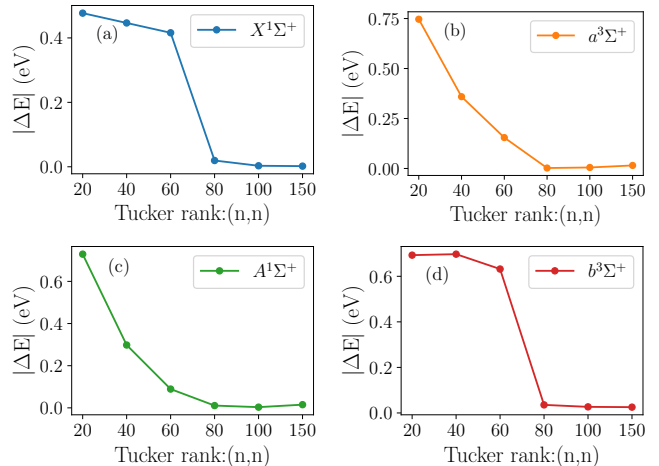


FIG. 4. Convergence of electronic eigenenergy (at 1.64 Å bond length) with different Tucker rank. Difference of calculated electronic energy from the FCI energy for the four electronic states (a) $X^1\Sigma^+$, (b) $a^3\Sigma^+$, (c) $A^1\Sigma^+$ and (d) $b^3\Sigma^+$ is shown.

orbitals are considered for the calculation. Three FS-DOFs are formed each consisting 4 spatial (or 8 spin) orbitals. We pruned the configurations in each FS-DOF following way: (i) In the first FS-DOF, we allow (2–4) alpha, (2–4) beta and (6–8) total electrons. (ii) In the second FS-DOF, we allow (0–2) alpha, (0–2) beta and

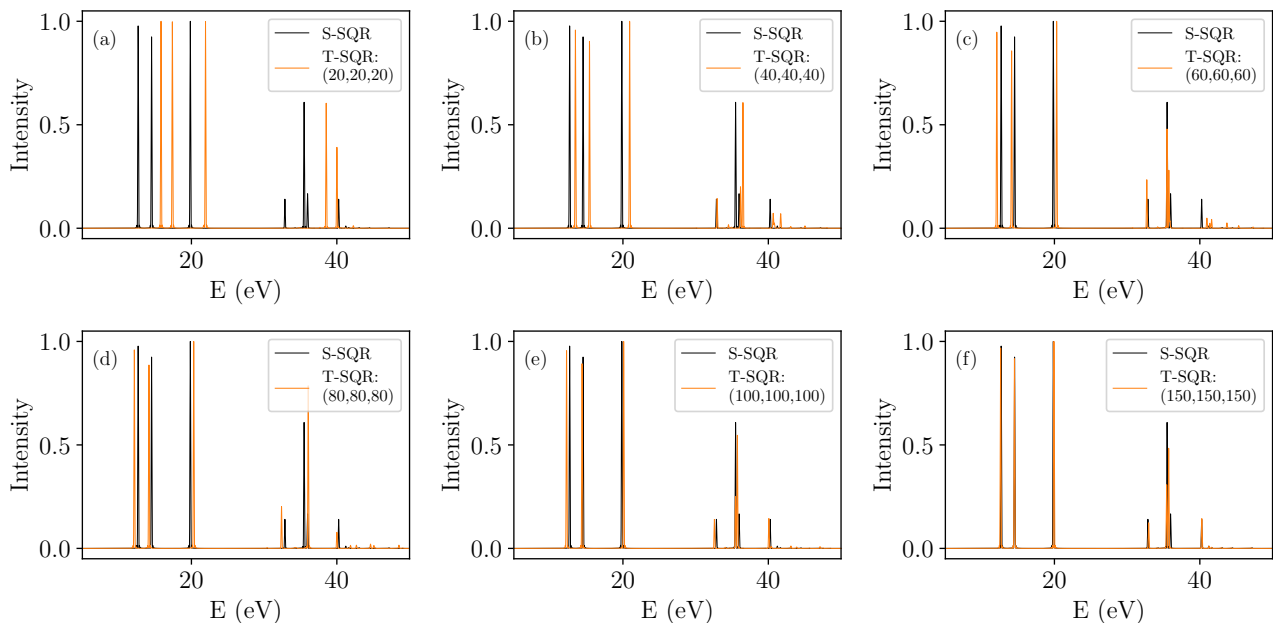


FIG. 5. Singly ionized states of H_2O with the T-SQR Hamiltonian approach. Electronic eigenenergies calculated with Tucker rank (20,20,20), (40,40,40), (60,60,60), (80,80,80), (100,100,100) and (150,150,150) are shown in (a), (b), (c), (d), (e) and (f), respectively. Maximum rank for the T-SQR Hamiltonian is (1369, 1369, 1369). The spectrum in black is calculated using the S-SQR Hamiltonian approach.

TABLE II. Number of Hamiltonian terms, memory required to store the operator matrices and wall-clock time for the different representation of the Hamiltonian. The wall-clock time is given for 20 fs time propagation. The calculations have been performed with 16 CPUs using shared-memory parallelization on the same machine and CPU type, namely, Dual-Core Intel Xeon, processor type E5-2650 v2 running at 2.6 GHz and the wall-clock times are intended for their relative comparison only. Maximum rank for the T-SQR Hamiltonian is (1369, 1369, 1369).

Method	Hamil. terms	Size	Time (h:m)
SQR	40618	200 KB	243:08
S-SQR	6890	5 MB	58:21
T-SQR			
(20, 20, 20)	800	7 MB	6:35
(40, 40, 40)	3200	11 MB	25:55
(60, 60, 60)	7200	26 MB	63:59
(80, 80, 80)	12800	82 MB	105:17
(100, 100, 100)	20000	90 MB	202:01
(150, 150, 150)	45000	132 MB	404:29

(0–2) total electrons and (iii) in the third FS-DOF, we allow (0–2) alpha, (0–2) beta and (0–2) total electrons. This generates 37 configurations in each of the three FS-DOFs. The electronic Hamiltonian is represented either

as S-SQR or T-SQR Hamiltonian approach. The initial wavefunction for the propagation is generated by applying ionization operator on the ground electronic state of neutral H_2O . The ionization operator reads

$$\hat{A} = \hat{a}_{1_\alpha} + \hat{a}_{1_\beta} + \hat{a}_{2_\alpha} + \hat{a}_{2_\beta} + \hat{a}_{3_\alpha} + \hat{a}_{3_\beta} + \hat{a}_{4_\alpha} + \hat{a}_{4_\beta}. \quad (25)$$

The initial wavefunction is spin doublet and overlaps with the singly ionized states of H_2O .

Table II compares the number of Hamiltonian terms, memory required to store the operator matrices and CPU time for different representations of the electronic Hamiltonian. We have presented two calculations with the exact Hamiltonian - one with the original SQR Hamiltonian and another with the S-SQR Hamiltonian where the correlated and uncorrelated operators are summed up as much as possible. This shows clear advantage of the S-SQR Hamiltonian over the original SQR Hamiltonian. Next, we represent the electronic Hamiltonian as T-SQR Hamiltonian with different Tucker rank. Fig. 5 compares the electronic ionization spectrum calculated using T-SQR Hamiltonian with S-SQR Hamiltonian. The convergence of the four main peaks of the singly ionized states calculated with different Tucker rank is shown in Fig. 6. It's clear that the convergence is achieved with a Tucker rank much smaller than the full rank (1369,1369,1369). However, here the S-SQR Hamiltonian achieves a more compact form of the SQR Hamiltonian than the converged calculation of comparable accuracy in the T-SQR approach.

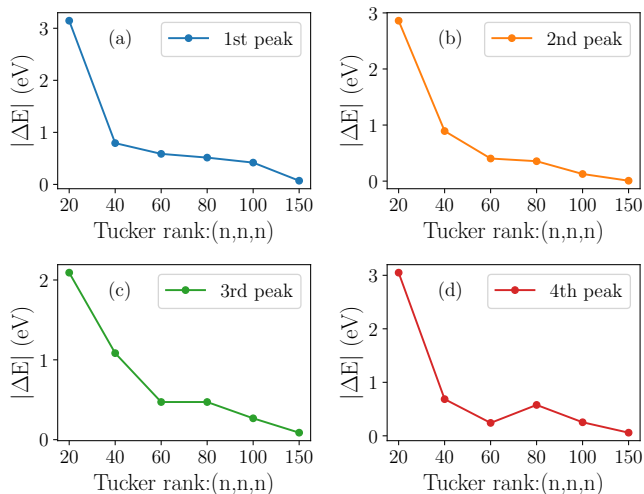


FIG. 6. Convergence of singly ionized state of H_2O with different Tucker rank. Difference of the electronic energies calculated with the T-SQR Hamiltonian from the S-SQR Hamiltonian for the 1st, 2nd, 3rd and 4th main peak centered around 12.7 eV, 14.5 eV, 19.8 eV and 35.5 eV is shown in (a), (b), (c) and (d), respectively.

The ionization spectrum is compared with the stick spectrum obtained from the third order algebraic diagrammatic construction ADC(3) method (Fig. 7). Two calculations in the SQR formalism are shown - one with the FS-DOF already mentioned before (SQR(small)) and another with the FS-DOF constructed as following (SQR(large)). Three FS-DOFs are formed each consisting 4 spatial (or 8 spin) orbitals. In the first FS-DOF, we allow (0–4) alpha, (0–4) beta and (4–8) total electrons and in the second and third FS-DOF, we allow (0–4) alpha, (0–4) beta and (0–4) total electrons. This generates 163 configurations in each of the three FS-DOFs. The improvement in the SQR(large) from the SQR(small) calculation is due to the larger sub-Fock space in each FS-DOF. The first three peaks represent the valance and core-valance ionization states of H_2O and correctly reproduced in the MCTDH-SQR calculation. The ionization from the core orbital produces several main and satellites states (spectrum above 30 eV). The small difference is due to the fact that the configuration space used in MCTDH-SQR method is different from the ADC(3) method. Formally, the intensity of the peaks in the normalized SQR spectrum is in the same limit as of the ADC(3) method. In both cases, the intensity represents the overlap of a ionized state with the corresponding one-hole ground state.

IV. SUMMARY AND CONCLUSIONS

In this work, we present a sum-of-products (SOP) form of the electronic Hamiltonian in the second quantized

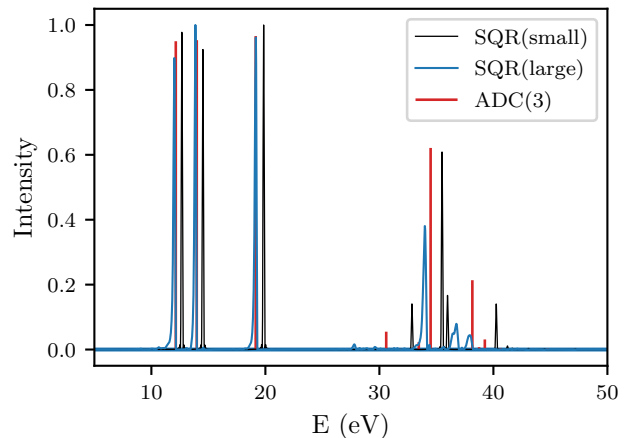


FIG. 7. Comparison of electronic ionization spectrum of H_2O with the stick spectrum obtained from the ADC(3) calculation. SQR(small) calculation is done by allowing (2–4) alpha, (2–4) beta and (6–8) total electrons in the first FS-DOF and (0–2) alpha, (0–2) beta and (0–2) total electrons in the 2nd and 3rd FS-DOF. SQR(large) calculation is done by allowing (0–4) alpha, (0–4) beta and (4–8) total electrons in the first FS-DOF and (0–4) alpha, (0–4) beta and (0–4) total electrons in the 2nd and 3rd FS-DOF.

representation (SQR). The N^4 scaling of the two-body part of the SQR electronic Hamiltonian with respect to the number of spin orbitals (N) poses a serious problem to study time dependent problems of large molecular systems. We formulate two approaches to circumvent this problem, where the primitive degrees of freedom (DOF) are represented as Fock-space DOF (FS-DOF). (i) First, each term of the original SQR Hamiltonian is represented in the sub-Fock space of the corresponding FS-DOF and then the correlated and uncorrelated terms are summed iteratively to form a more compact SOP form of the SQR Hamiltonian (S-SQR Hamiltonian). One obtains the most compact and still exact form of the electronic Hamiltonian once all terms that could be summed have been identified. Further compactification within this strategy can only be achieved by setting a cutoff value for the one- and two-body integrals. This shows its intrinsic limitation as a compactification method. (ii) Second, the electronic Hamiltonian is assumed to have a Tucker tensor form (T-SQR Hamiltonian) and the task is to obtain the optimal core tensor and single particle operator (SPO) matrices that minimize the difference to the exact Hamiltonian. Usually as the Tucker rank is much smaller than the rank of the original Hamiltonian, one achieves a more compact SOP form of the Hamiltonian than the original tensor.

As a proof-of-concept, we apply these two approaches to calculate the potential energy curves (PECs) of the four lowest lying electronic states of LiH and electronic ionization spectrum of H_2O . In these two numerical examples, we compare the convergence of the electronic

eigen energies with respect to the Tucker rank. As expected, the accuracy of the obtained results increases as the Tucker rank grows and the numerically converged form of the electronic Hamiltonian can be achieved with fewer product terms (lower Tucker rank) compared to the rank of the original Hamiltonian tensor. For LiH, the converged calculation of comparable accuracy in the T-SQR Hamiltonian approach outperforms the S-SQR Hamiltonian approach. For the H₂O example, the S-SQR Hamiltonian achieves a more compact form of the Hamiltonian than the converged calculation of T-SQR Hamiltonian. We believe that in problems with a larger number of FS-DOF this trend will be overturned and the numerically optimized SOP form will be the most efficient one.

We emphasize here that our goal has been to establish whether the electronic Hamiltonian can be systematically approximated as a SOP with an increasing accuracy as a function of the Tucker expansion rank, and found that this is indeed the case. We defer to future work finding practical ways to generate SOP forms for the electronic Hamiltonian for cases where the primitive tensor operator is too large for a direct decomposition in Tucker form. For example, the exponential scaling with respect to the Tucker rank can be avoided by using approximations based on the canonical polyadic decomposition (also known as PARAFAC or CANDECOMP in literature) of the Hamiltonian tensor. This strategy is very successful in representing the multi-dimensional potential energy surfaces into SOP form⁴³, which might be extendable to the electronic problem.

V. SUPPLEMENTARY MATERIAL

See the supplementary material for the tabular data of the potential energy curves of LiH, ionization energies of H₂O.

VI. DATA AVAILABILITY

The data that support the findings of this study are available in tabular form in the supplementary materials.

VII. ACKNOWLEDGMENTS

We thank Prof. H.-D. Meyer for his important assistance with the MCTDH calculations. The authors thank JUSTUS 2 in Ulm for computing time. The authors declare no conflicts of interest.

Appendix A: Compacted form of the electronic Hamiltonian in the spin orbital basis

The electronic Hamiltonian written in Eq. 7 reads as

$$\hat{H}_{el} = \hat{H}_1 + \hat{H}_2, \quad (\text{A1})$$

where

$$\begin{aligned} \hat{H}_1 &= \sum_{ij} h_{ij} \left(\prod_{q=a+1}^{b-1} \hat{\sigma}_q^z \right) \hat{\sigma}_i^+ \hat{\sigma}_j^- \\ &= \sum_{ij} h_{ij} \hat{O}_{ij}, \end{aligned} \quad (\text{A2})$$

and

$$\begin{aligned} \hat{H}_2 &= \frac{1}{2} \sum_{ijkl} v_{ijkl} \left(\prod_{q=a+1}^{b-1} \hat{\sigma}_q^z \prod_{q'=c+1}^{d-1} \hat{\sigma}_{q'}^z \right) \\ &\quad \text{sgn}(j-i) \text{sgn}(l-k) \hat{\sigma}_i^+ \hat{\sigma}_j^+ \hat{\sigma}_l^- \hat{\sigma}_k^- \\ &= \sum_{ijkl} v_{ijkl} \hat{O}_{ijkl}. \end{aligned} \quad (\text{A3})$$

Here, \hat{O}_{ij} and \hat{O}_{ijkl} denote the entire operator form of the 1e- and 2e-part of Eqs. A2 and A2, respectively. Now, one can divide the Hamiltonian by the index of the orbital belongs to their corresponding FS-DOF.

$$\hat{H}_1 = \sum_{\alpha}^f \sum_{i_{\alpha} j_{\alpha}}^{m_{\alpha}} h_{i_{\alpha} j_{\alpha}} \hat{O}_{i_{\alpha} j_{\alpha}} + \sum_{\alpha < \beta}^f \mathbf{P}(\alpha, \beta) \sum_{i_{\alpha}}^{m_{\alpha}} \sum_{j_{\beta}}^{m_{\beta}} h_{i_{\alpha} j_{\beta}} \hat{O}_{i_{\alpha} j_{\beta}}, \quad (\text{A4})$$

where i_{κ} denotes the index of the orbital of the κ -th FS-DOF and m_{κ} is the number of spin orbitals grouped to form the κ -th FS-DOF and f is the number of FS-DOFs under consideration. $\mathbf{P}(\alpha, \beta)$ is the permutation operator that generates all the possible permutation of the indices

$$\mathbf{P}(\alpha, \beta) X(\alpha, \beta) = X(\alpha, \beta) + X(\beta, \alpha). \quad (\text{A5})$$

Now, one can divide the operator $\hat{O}_{i_{\alpha} j_{\beta}}$ into sub-operators that act only on the corresponding FS-DOF. The one-body part of the Hamiltonian reads

$$\begin{aligned}
\hat{H}_1 &= \sum_{\alpha}^f \sum_{i_{\alpha} j_{\alpha}}^{m_{\alpha}} h_{i_{\alpha} j_{\alpha}} \hat{O}_{i_{\alpha} j_{\alpha}}^{(\alpha)} + \sum_{\alpha < \beta}^f \mathbf{P}(\alpha, \beta) \sum_{i_{\alpha}}^{m_{\alpha}} \sum_{j_{\beta}}^{m_{\beta}} h_{i_{\alpha} j_{\beta}} \hat{O}_{i_{\alpha}}^{(\alpha)} \hat{O}^{(\alpha+1)} \dots \hat{O}^{(\beta-1)} \hat{O}_{j_{\beta}}^{(\beta)} \\
&= \sum_{\alpha}^f \left(\sum_{i_{\alpha} j_{\alpha}}^{m_{\alpha}} h_{i_{\alpha} j_{\alpha}} \hat{O}_{i_{\alpha} j_{\alpha}}^{(\alpha)} \right) + \sum_{\alpha < \beta}^f \mathbf{P}(\alpha, \beta) \sum_{i_{\alpha}}^{m_{\alpha}} \hat{O}_{i_{\alpha}}^{(\alpha)} \hat{O}^{(\alpha+1)} \dots \hat{O}^{(\beta-1)} \left(\sum_{j_{\beta}}^{m_{\beta}} h_{i_{\alpha} j_{\beta}} \hat{O}_{j_{\beta}}^{(\beta)} \right). \quad (\text{A6})
\end{aligned}$$

Here, $\hat{O}_{a_{\kappa} b_{\kappa} \dots}^{(\kappa)}$ denotes an operator string consists of spin ladder operators of $(a_{\kappa}, b_{\kappa}, \dots)$ orbitals and sign change or identity operator of other orbitals of the κ -th FS-

DOF. \hat{O}^{κ} denotes an operator string consists of either sign change or identity operator of the spin orbitals of κ -th FS-DOF. Similarly, the two-body part of the Hamiltonian reads

$$\begin{aligned}
\hat{H}_2 &= \sum_{ijkl} v_{ijkl} \hat{O}_{ijkl} \\
&= \sum_{\alpha}^f \sum_{i_{\alpha} j_{\alpha} k_{\alpha} l_{\alpha}}^{m_{\alpha}} v_{i_{\alpha} j_{\alpha} k_{\alpha} l_{\alpha}} \hat{O}_{i_{\alpha} j_{\alpha} k_{\alpha} l_{\alpha}}^{(\alpha)} \\
&+ \sum_{\alpha < \beta}^f \mathbf{P}(\alpha, \alpha, \alpha, \beta) \sum_{i_{\alpha} j_{\alpha} k_{\alpha}}^{m_{\alpha}} \sum_{l_{\beta}}^{m_{\beta}} v_{i_{\alpha} j_{\alpha} k_{\alpha} l_{\beta}} \hat{O}_{i_{\alpha} j_{\alpha} k_{\alpha}}^{(\alpha)} \hat{O}^{(\alpha+1)} \dots \hat{O}^{(\beta-1)} \hat{O}_{l_{\beta}}^{(\beta)} \\
&+ \sum_{\alpha < \beta}^f \mathbf{P}(\alpha, \alpha, \beta, \beta) \sum_{i_{\alpha} j_{\alpha}}^{m_{\alpha}} \sum_{k_{\beta} l_{\beta}}^{m_{\beta}} v_{i_{\alpha} j_{\alpha} k_{\beta} l_{\beta}} \hat{O}_{i_{\alpha} j_{\alpha}}^{(\alpha)} \hat{O}_{k_{\beta} l_{\beta}}^{(\beta)} \\
&+ \sum_{\alpha < \beta < \gamma}^f \mathbf{P}(\alpha, \alpha, \beta, \gamma) \sum_{i_{\alpha} j_{\alpha}}^{m_{\alpha}} \sum_{k_{\beta}}^{m_{\beta}} \sum_{l_{\gamma}}^{m_{\gamma}} v_{i_{\alpha} j_{\alpha} k_{\beta} l_{\gamma}} \hat{O}_{i_{\alpha} j_{\alpha}}^{(\alpha)} \hat{O}_{k_{\beta}}^{(\beta)} \hat{O}^{(\beta+1)} \dots \hat{O}^{(\gamma-1)} \hat{O}_{l_{\gamma}}^{(\gamma)} \\
&+ \sum_{\alpha < \beta < \gamma < \delta}^f \mathbf{P}(\alpha, \beta, \gamma, \delta) \sum_{i_{\alpha}}^{m_{\alpha}} \sum_{j_{\beta}}^{m_{\beta}} \sum_{k_{\gamma}}^{m_{\gamma}} \sum_{l_{\delta}}^{m_{\delta}} v_{i_{\alpha} j_{\beta} k_{\gamma} l_{\delta}} \hat{O}_{i_{\alpha}}^{(\alpha)} \hat{O}^{(\alpha+1)} \dots \hat{O}^{(\beta-1)} \hat{O}_{j_{\beta}}^{(\beta)} \hat{O}_{k_{\gamma}}^{(\gamma)} \hat{O}^{(\gamma+1)} \dots \hat{O}^{(\delta-1)} \hat{O}_{l_{\delta}}^{(\delta)} \\
&= \sum_{\alpha}^f \left(\sum_{i_{\alpha} j_{\alpha} k_{\alpha} l_{\alpha}}^{m_{\alpha}} v_{i_{\alpha} j_{\alpha} k_{\alpha} l_{\alpha}} \hat{O}_{i_{\alpha} j_{\alpha} k_{\alpha} l_{\alpha}}^{(\alpha)} \right) \\
&+ \sum_{\alpha < \beta}^f \mathbf{P}(\alpha, \alpha, \alpha, \beta) \left(\sum_{i_{\alpha} j_{\alpha} k_{\alpha}}^{m_{\alpha}} v_{i_{\alpha} j_{\alpha} k_{\alpha} l_{\beta}} \hat{O}_{i_{\alpha} j_{\alpha} k_{\alpha}}^{(\alpha)} \right) \hat{O}^{(\alpha+1)} \dots \hat{O}^{(\beta-1)} \sum_{l_{\beta}}^{m_{\beta}} \hat{O}_{l_{\beta}}^{(\beta)} \\
&+ \sum_{\alpha < \beta}^f \mathbf{P}(\alpha, \alpha, \beta, \beta) \sum_{i_{\alpha} j_{\alpha}}^{m_{\alpha}} \hat{O}_{i_{\alpha} j_{\alpha}}^{(\alpha)} \left(\sum_{k_{\beta} l_{\beta}}^{m_{\beta}} v_{i_{\alpha} j_{\alpha} k_{\beta} l_{\beta}} \hat{O}_{k_{\beta} l_{\beta}}^{(\beta)} \right) \\
&+ \sum_{\alpha < \beta < \gamma}^f \mathbf{P}(\alpha, \alpha, \beta, \gamma) \left(\sum_{i_{\alpha} j_{\alpha}}^{m_{\alpha}} v_{i_{\alpha} j_{\alpha} k_{\beta} l_{\gamma}} \hat{O}_{i_{\alpha} j_{\alpha}}^{(\alpha)} \right) \sum_{k_{\beta}}^{m_{\beta}} \sum_{l_{\gamma}}^{m_{\gamma}} \hat{O}_{k_{\beta}}^{(\beta)} \hat{O}^{(\beta+1)} \dots \hat{O}^{(\gamma-1)} \hat{O}_{l_{\gamma}}^{(\gamma)} \\
&+ \sum_{\alpha < \beta < \gamma < \delta}^f \mathbf{P}(\alpha, \beta, \gamma, \delta) \sum_{i_{\alpha}}^{m_{\alpha}} \sum_{j_{\beta}}^{m_{\beta}} \sum_{k_{\gamma}}^{m_{\gamma}} \hat{O}_{i_{\alpha}}^{(\alpha)} \hat{O}^{(\alpha+1)} \dots \hat{O}^{(\beta-1)} \hat{O}_{j_{\beta}}^{(\beta)} \hat{O}_{k_{\gamma}}^{(\gamma)} \hat{O}^{(\gamma+1)} \dots \hat{O}^{(\delta-1)} \left(\sum_{l_{\delta}}^{m_{\delta}} v_{i_{\alpha} j_{\beta} k_{\gamma} l_{\delta}} \hat{O}_{l_{\delta}}^{(\delta)} \right). \quad (\text{A7})
\end{aligned}$$

Here, we can sum the terms in the parenthesis as they

act only on one primitive DOF to reduce the number of

Hamiltonian terms.

Appendix B: Application of Hamiltonian on the wavefunction: Matrix vs Mapping

The operators acting on the SPFs of the FS-DOF are very sparse as each term the electronic Hamiltonian given in Eq. 7 can connect one bra configuration of the FS-DOF to only one specific ket configuration of the corresponding FS-DOF. Thus, the matrix operators have the property that at most there is one non-zero entry in each row and column that can be either equal to 1 or -1. As a consequence, for an $(m \times m)$ matrix, at most m entries are different from 0. This sparsity can be exploited by matrix-vector multiplication algorithms with linear rather than quadratic scaling. For example, $a_1^\dagger a_4$ operator term is applied to a sequence of four combined S-DOFs as

$$a_1^\dagger a_4 = \sigma_1^\dagger S_2 S_3 \sigma_4 = \begin{pmatrix} 0 & 0 \\ 1 & 0 \end{pmatrix}_{(1)} \begin{pmatrix} 1 & 0 \\ 0 & -1 \end{pmatrix}_{(2)} \begin{pmatrix} 1 & 0 \\ 0 & -1 \end{pmatrix}_{(3)} \begin{pmatrix} 0 & 1 \\ 0 & 0 \end{pmatrix}_{(4)}. \quad (\text{B1})$$

The same operator in the FS-DOF sub-Fock space reads

$$a_1^\dagger a_4 = \sigma_1^\dagger S_2 S_3 \sigma_4 = \begin{pmatrix} 0 & 0 & 0 & 0 & 0 & 0 & 0 & 0 & 0 & 0 & 0 & 0 & 0 & 0 & 0 & 0 & 0 & 0 & 0 & 0 \\ 0 & 0 & 0 & 0 & 0 & 0 & 0 & 0 & 0 & 0 & 0 & 0 & 0 & 0 & 0 & 0 & 0 & 0 & 0 & 0 \\ 0 & 0 & 0 & 1 & 0 & 0 & 0 & 0 & 0 & 0 & 0 & 0 & 0 & 0 & 0 & 0 & 0 & 0 & 0 & 0 \\ 0 & 0 & 0 & 0 & 0 & 0 & 0 & 0 & 0 & 0 & 0 & 0 & 0 & 0 & 0 & 0 & 0 & 0 & 0 & 0 \\ 0 & 0 & 0 & 0 & 0 & 0 & 0 & 0 & 0 & 0 & 0 & 0 & 0 & 0 & 0 & 0 & 0 & 0 & 0 & 0 \\ 0 & 0 & 0 & 0 & 0 & 0 & -1 & 0 & 0 & 0 & 0 & 0 & 0 & 0 & 0 & 0 & 0 & 0 & 0 & 0 \\ 0 & 0 & 0 & 0 & 0 & 0 & 0 & 0 & 0 & 0 & 0 & 0 & 0 & 0 & 0 & 0 & 0 & 0 & 0 & 0 \\ 0 & 0 & 0 & 0 & 0 & 0 & 0 & 0 & 0 & 0 & 0 & 0 & 0 & 0 & 0 & 0 & 0 & 0 & 0 & 0 \\ 0 & 0 & 0 & 0 & 0 & 0 & 0 & 0 & 0 & 0 & 0 & 0 & 0 & 0 & 0 & 0 & 0 & 0 & 0 & 0 \\ 0 & 0 & 0 & 0 & 0 & 0 & 0 & 0 & 0 & 0 & 0 & 0 & 0 & 0 & 0 & 0 & 0 & 0 & 0 & 0 \\ 0 & 0 & 0 & 0 & 0 & 0 & 0 & 0 & 0 & 0 & 0 & 0 & 0 & 0 & 0 & 0 & 0 & 0 & 0 & 0 \\ 0 & 0 & 0 & 0 & 0 & 0 & 0 & 0 & 0 & 0 & 0 & 0 & 0 & 0 & 0 & 0 & 0 & 0 & 0 & 0 \\ 0 & 0 & 0 & 0 & 0 & 0 & 0 & 0 & 0 & 0 & 0 & 0 & 0 & 0 & 0 & 0 & 0 & 0 & 0 & 0 \\ 0 & 0 & 0 & 0 & 0 & 0 & 0 & 0 & 0 & 0 & 0 & 0 & 0 & 0 & 0 & 0 & 0 & 0 & 0 & 0 \\ 0 & 0 & 0 & 0 & 0 & 0 & 0 & 0 & 0 & 0 & 0 & 0 & 0 & 0 & 0 & 0 & 0 & 0 & 0 & 0 \\ 0 & 0 & 0 & 0 & 0 & 0 & 0 & 0 & 0 & 0 & 0 & 0 & 0 & 0 & 0 & 0 & 0 & 0 & 0 & 0 \\ 0 & 0 & 0 & 0 & 0 & 0 & 0 & 0 & 0 & 0 & 0 & 0 & 0 & 0 & 0 & 0 & 0 & 0 & 0 & 0 \\ 0 & 0 & 0 & 0 & 0 & 0 & 0 & 0 & 0 & 0 & 0 & 0 & 0 & 0 & 0 & 0 & 0 & 0 & 0 & 0 \end{pmatrix}. \quad (\text{B2})$$

So, the application of this operator to the SPFs of the FS-DOF operator is a mapping where only certain memory positions need to be copied

$$\begin{pmatrix} 0 & 0 & 0 & 0 & 0 & 0 & 0 & 0 & 0 & 0 & 0 & 0 & 0 & 0 & 0 & 0 & 0 & 0 & 0 & 0 \\ 0 & 0 & 0 & 0 & 0 & 0 & 0 & 0 & 0 & 0 & 0 & 0 & 0 & 0 & 0 & 0 & 0 & 0 & 0 & 0 \\ 0 & 0 & 0 & 1 & 0 & 0 & 0 & 0 & 0 & 0 & 0 & 0 & 0 & 0 & 0 & 0 & 0 & 0 & 0 & 0 \\ 0 & 0 & 0 & 0 & 0 & 0 & 0 & 0 & 0 & 0 & 0 & 0 & 0 & 0 & 0 & 0 & 0 & 0 & 0 & 0 \\ 0 & 0 & 0 & 0 & 0 & 0 & 0 & 0 & 0 & 0 & 0 & 0 & 0 & 0 & 0 & 0 & 0 & 0 & 0 & 0 \\ 0 & 0 & 0 & 0 & 0 & 0 & -1 & 0 & 0 & 0 & 0 & 0 & 0 & 0 & 0 & 0 & 0 & 0 & 0 & 0 \\ 0 & 0 & 0 & 0 & 0 & 0 & 0 & 0 & 0 & 0 & 0 & 0 & 0 & 0 & 0 & 0 & 0 & 0 & 0 & 0 \\ 0 & 0 & 0 & 0 & 0 & 0 & 0 & 0 & 0 & 0 & 0 & 0 & 0 & 0 & 0 & 0 & 0 & 0 & 0 & 0 \\ 0 & 0 & 0 & 0 & 0 & 0 & 0 & 0 & 0 & 0 & 0 & 0 & 0 & 0 & 0 & 0 & 0 & 0 & 0 & 0 \\ 0 & 0 & 0 & 0 & 0 & 0 & 0 & 0 & 0 & 0 & 0 & 0 & 0 & 0 & 0 & 0 & 0 & 0 & 0 & 0 \\ 0 & 0 & 0 & 0 & 0 & 0 & 0 & 0 & 0 & 0 & 0 & 0 & 0 & 0 & 0 & 0 & 0 & 0 & 0 & 0 \\ 0 & 0 & 0 & 0 & 0 & 0 & 0 & 0 & 0 & 0 & 0 & 0 & 0 & 0 & 0 & 0 & 0 & 0 & 0 & 0 \\ 0 & 0 & 0 & 0 & 0 & 0 & 0 & 0 & 0 & 0 & 0 & 0 & 0 & 0 & 0 & 0 & 0 & 0 & 0 & 0 \\ 0 & 0 & 0 & 0 & 0 & 0 & 0 & 0 & 0 & 0 & 0 & 0 & 0 & 0 & 0 & 0 & 0 & 0 & 0 & 0 \\ 0 & 0 & 0 & 0 & 0 & 0 & 0 & 0 & 0 & 0 & 0 & 0 & 0 & 0 & 0 & 0 & 0 & 0 & 0 & 0 \\ 0 & 0 & 0 & 0 & 0 & 0 & 0 & 0 & 0 & 0 & 0 & 0 & 0 & 0 & 0 & 0 & 0 & 0 & 0 & 0 \\ 0 & 0 & 0 & 0 & 0 & 0 & 0 & 0 & 0 & 0 & 0 & 0 & 0 & 0 & 0 & 0 & 0 & 0 & 0 & 0 \\ 0 & 0 & 0 & 0 & 0 & 0 & 0 & 0 & 0 & 0 & 0 & 0 & 0 & 0 & 0 & 0 & 0 & 0 & 0 & 0 \end{pmatrix} \begin{pmatrix} a_1 \\ a_2 \\ a_3 \\ a_4 \\ a_5 \\ a_6 \\ a_7 \\ a_8 \\ a_9 \\ a_{10} \\ a_{11} \\ a_{12} \\ a_{13} \\ a_{14} \\ a_{15} \\ a_{16} \end{pmatrix} = \begin{pmatrix} 0 \\ 0 \\ a_4 \\ 0 \\ 0 \\ -a_7 \\ 0 \\ 0 \\ 0 \\ -a_{11} \\ 0 \\ 0 \\ a_{14} \\ 0 \\ 0 \\ 0 \\ 0 \\ 0 \\ 0 \\ 0 \end{pmatrix}. \quad (\text{B3})$$

In this case, instead of 16^2 floating point operations (FLOP), the mapping strategy requires just 4 FLOPs. Another advantage of the mapping algorithm is that one requires significantly less memory for the matrix-vector multiplication – i.e., only the indices of rows, columns and the sign of the non-zero matrix elements need to be stored instead of the full matrix. The pseudo-code for the mapping algorithm is given in Algorithm 1. This has

Algorithm 1: Mapping algorithm

Input : Arrays: $\mathbf{row}(i)$, $\mathbf{col}(i)$, $\mathbf{sgn}(i)$, $\mathbf{ovec}(i)$,
 $i = 1, 2, \dots, n$, where each element of \mathbf{row}
and \mathbf{col} is integer, \mathbf{ovec} is real/complex and
 \mathbf{sgn} is either 1 or -1 . \mathbf{row} , \mathbf{col} , \mathbf{sgn} stores
the indices of row and column and sign of
the non-zero matrix elements of the
operator, respectively. \mathbf{ovec} stores the
coefficients of vector before multiplication.
Output: Array: $\mathbf{nvec}(i)$, $i = 1, 2, \dots, m$, where each
element of \mathbf{nvec} is a real/complex. \mathbf{nvec}
stores the resulting vector of the
matrix-vector multiplication.

```

/* Initialization of nvec as zero */
nvec = 0.0
/* map the elements of nvec to the elements of
   ovec with proper sign */
for i ← 0 to n do
| nvec(row(i)) = sgn(i) * ovec(col(i))
end for

```

been implemented in the Heidelberg MCTDH package and can be switched on whenever very sparse operators are encountered for any degree of freedom, not only in the MCTDH-SQR context.

- ¹H. D. Meyer, U. Manthe, and L. S. Cederbaum, *Chem. Phys. Lett.* **165**, 73 (1990).
- ²U. Manthe, H.-D. Meyer, and L. S. Cederbaum, *J. Chem. Phys.* **97**, 3199 (1992).
- ³M. H. Beck, A. Jäckle, G. A. Worth, and H.-D. Meyer, *Phys. Rep.* **324**, 1 (2000).
- ⁴H.-D. Meyer and G. A. Worth, *Theor. Chem. Acc.* **109**, 251 (2003).
- ⁵H.-D. Meyer, F. Gatti, and G. A. Worth, eds., *Multidimensional Quantum Dynamics* (Wiley, 2009).
- ⁶H. Wang and M. Thoss, *J. Chem. Phys.* **119**, 1289 (2003).
- ⁷U. Manthe, *J. Chem. Phys.* **128**, 164116 (2008).
- ⁸O. Vendrell and H.-D. Meyer, *J. Chem. Phys.* **134**, 044135 (2011).
- ⁹H.-D. Meyer, *WIREs Comput Mol Sci* **2**, 351 (2012).
- ¹⁰H. Wang, *J. Phys. Chem. A* **119**, 7951 (2015).
- ¹¹J. Caillat, J. Zanghellini, M. Kitzler, O. Koch, W. Kreuzer, and A. Scrinzi, *Phys. Rev. A* **71**, 012712 (2005).
- ¹²O. E. Alon, A. I. Streltsov, and L. S. Cederbaum, *J. Chem. Phys.* **127**, 154103 (2007).
- ¹³D. Hochstuhl and M. Bonitz, *J. Chem. Phys.* **134**, 084106 (2011).
- ¹⁴T. Sato and K. L. Ishikawa, *Phys. Rev. A* **88**, 023402 (2013).
- ¹⁵A. U. Lode, C. Lévéque, L. B. Madsen, A. I. Streltsov, and O. E. Alon, *Rev. Mod. Phys.* **92**, 011001 (2020).
- ¹⁶O. E. Alon, A. I. Streltsov, and L. S. Cederbaum, *Phys. Rev. A* **77**, 033613 (2008).
- ¹⁷S. Krönke, L. Cao, O. Vendrell, and P. Schmelcher, *New J. Phys.* **15**, 063018 (2013).
- ¹⁸H. Wang and M. Thoss, *J. Chem. Phys.* **131**, 024114 (2009).

- ¹⁹K. Balzer, Z. Li, O. Vendrell, and M. Eckstein, *Phys. Rev. B* **91**, 045136 (2015).
- ²⁰H. Wang, I. Pshenichnyuk, R. Härtle, and M. Thoss, *J. Chem. Phys.* **135**, 244506 (2011).
- ²¹H. Wang and M. Thoss, *J. Chem. Phys.* **138**, 134704 (2013).
- ²²H. Wang and M. Thoss, *J. Phys. Chem. A* **117**, 7431 (2013).
- ²³E. Y. Wilner, H. Wang, G. Cohen, M. Thoss, and E. Rabani, *Phys. Rev. B* **88**, 045137 (2013).
- ²⁴E. Y. Wilner, H. Wang, M. Thoss, and E. Rabani, *Phys. Rev. B* **89**, 205129 (2014).
- ²⁵U. Manthe and T. Weike, *J. Chem. Phys.* **146**, 064117 (2017).
- ²⁶T. Weike and U. Manthe, *J. Chem. Phys.* **152**, 034101 (2020).
- ²⁷S. Sasmal and O. Vendrell, *J. Chem. Phys.* **153**, 154110 (2020).
- ²⁸S. R. White, *Physical Review Letters* **69**, 2863 (1992).
- ²⁹S. R. White, *Physical Review B* **48**, 10345 (1993).
- ³⁰U. Schollwoeck, *Rev. Mod. Phys.* **77**, 259 (2005).
- ³¹U. Schollwöck, *Annals of Physics* **326**, 96 (2011).
- ³²G. K.-L. Chan and S. Sharma, *Annual Review of Physical Chemistry* **62**, 465 (2011).
- ³³I. P. McCulloch, *Journal of Statistical Mechanics: Theory and Experiment* **2007**, P10014 (2007).
- ³⁴G. K.-L. Chan, A. Keselman, N. Nakatani, Z. Li, and S. R. White, *J. Chem. Phys.* **145**, 014102 (2016).
- ³⁵S. Keller, M. Dolfi, M. Troyer, and M. Reiher, *J. Chem. Phys.* **143**, 244118 (2015).
- ³⁶T. Yanai, Y. Kurashige, W. Mizukami, J. Chalupský, T. N. Lan, and M. Saitow, *International Journal of Quantum Chemistry* **115**, 283 (2014).
- ³⁷A. Jäckle and H.-D. Meyer, *J. Chem. Phys.* **104**, 7974 (1996).
- ³⁸A. Jäckle and H.-D. Meyer, *J. Chem. Phys.* **109**, 3772 (1998).
- ³⁹D. Peláez and H.-D. Meyer, *J. Chem. Phys.* **138**, 014108 (2013).
- ⁴⁰M. Schröder and H.-D. Meyer, *J. Chem. Phys.* **147**, 064105 (2017).
- ⁴¹F. Otto, Y.-C. Chiang, and D. Peláez, *Chemical Physics* **509**, 116 (2018).
- ⁴²F. Otto, *J. Chem. Phys.* **140**, 014106 (2014).
- ⁴³M. Schröder, *J. Chem. Phys.* **152**, 024108 (2020).
- ⁴⁴S. Manzhos, X. Wang, R. Dawes, and T. Carrington, *J. Phys. Chem. A* **110**, 5295 (2005).
- ⁴⁵S. Manzhos and T. Carrington, *J. Chem. Phys.* **125**, 084109 (2006).
- ⁴⁶S. Manzhos and T. Carrington, *J. Chem. Phys.* **125**, 194105 (2006).
- ⁴⁷W. Koch and D. H. Zhang, *J. Chem. Phys.* **141**, 021101 (2014).
- ⁴⁸X. Shen, J. Chen, Z. Zhang, K. Shao, and D. H. Zhang, *J. Chem. Phys.* **143**, 144701 (2015).
- ⁴⁹E. Pradhan and A. Brown, *J. Chem. Phys.* **144**, 174305 (2016).
- ⁵⁰E. Pradhan and A. Brown, *Journal of Molecular Spectroscopy* **330**, 158 (2016).
- ⁵¹A. L. Fetter and J. D. Walecka, *Quantum Theory of Many-Particle Systems* (Dover Publications Inc., 2003).
- ⁵²P. Jordan and E. Wigner, *Zeitschrift für Physik* **47**, 631 (1928).
- ⁵³F. L. Hitchcock, *Journal of Mathematics and Physics* **6**, 164 (1927).
- ⁵⁴R. A. Harshman, *UCLA Working Papers in Phonetics* **16**, 1 (1970).
- ⁵⁵J. D. Carroll and J.-J. Chang, *Psychometrika* **35**, 283 (1970).
- ⁵⁶H. A. L. Kiers, *Journal of Chemometrics* **14**, 105 (2000).
- ⁵⁷J. C. Slater, *Physical Review* **34**, 1293 (1929).
- ⁵⁸E. U. Condon, *Physical Review* **36**, 1121 (1930).
- ⁵⁹J. Kossaifi, Y. Panagakis, A. Anandkumar, and M. Pantic, *Journal of Machine Learning Research* **20**, 1 (2019).
- ⁶⁰T. G. Kolda and B. W. Bader, *SIAM Rev* **51**, 455 (2009).
- ⁶¹G. A. Worth, M. H. Beck, A. Jäckle, O. Vendrell, and H.-D. Meyer, The MCTDH Package, Version 8.2, (2000). H.-D. Meyer, Version 8.3 (2002), Version 8.4 (2007). O. Vendrell and H.-D. Meyer Version 8.5 (2013). Version 8.5 contains the ML-MCTDH algorithm. Current versions: 8.4.18 and 8.5.11 (2019). Used version: exchange with "Used version" See <http://mctdh.uni-hd.de/>.